Direct Observations of Structural Phases in Crystallized Ion Plasmas

T. B. Mitchell*, J. J. Bollinger, X.-P. Huang and W. M. Itano
Time and Frequency Division, National Institute of Standards and Technology, Boulder, CO 80303

D. H. E. Dubin
Department of Physics, University of California at San Diego, La Jolla, CA 92093

Laser-cooled $^9Be^+$ ions confined in a Penning-Malmberg trap were directly observed, and the images were used to characterize the structural phases of the ions. With the ions in two-dimensionally extended lattice planes, five different stable crystalline phases were observed, and the energetically favored structure could be sensitively tuned by changing the areal density of the confined ions. Qualitatively similar structural phase transitions occur, or are predicted to occur, in other planar single-component systems with a variety of interparticle interactions. Closed shell structures were observed with small ion clouds that were spherical or prolate, and crystals with long range order were observed in the centers of clouds with large numbers of ions. These experimental results are in good agreement with theoretical predictions for the strongly coupled one-component plasma.

I. INTRODUCTION

The one-component plasma (OCP) has been a model of condensed matter in statistical physics for over 60 years, and it is used to describe such diverse systems as dense astrophysical matter [1] and electrons on the surface of liquid helium [2]. Laser-cooled trapped ions [3] are an excellent experimental realization of the OCP. The phase structures of spatially homogeneous (infinite) [4,5], cylindrical (infinite in one dimension only) [6,7], and planar (with up to 5 planes) [8] OCPs have been explored previously using Bragg diffraction and direct imaging. Here, images of ions that were confined in planar, cylindrical, and spatially homogeneous geometries in a Penning trap are presented and used to characterize the structural phases. The observed structures agree well with the theoretical predictions for the OCP.

The OCP model consists of a single charged species embedded in a uniform, neutralizing background charge. In Paul [9] or Penning [9,10] traps, which are used to confine charged particles, a (fictitious) neutralizing background is provided by the confining potentials. The thermodynamic properties of the infinite classical OCP are determined by its Coulomb coupling parameter,

$$\Gamma \equiv \frac{1}{4\pi\epsilon_0}\frac{e^2}{a_{WS}k_BT}, \qquad (1)$$

which is the ratio of the Coulomb potential energy of neighboring ions to the kinetic energy per ion. Here, ϵ_0 is the permittivity of the vacuum, e is the charge of an ion, k_B is Boltzmann's constant, T is the temperature, and a_{ws} is the Wigner-Seitz radius, defined by $4\pi(a_{ws})^3/3 = 1/n_0$ where n_0 is the ion density. The onset of short-range order for the infinite OCP is predicted [11] at $\Gamma \approx 2$, and a phase transition to a body-centered cubic (bcc) lattice is predicted [11–13] at $\Gamma \approx 170$. With an OCP in a planar geometry (infinite in only two directions), boundary effects are predicted to cause the formation of a variety of additional structural phases, such as the hexagonal close-packed (hcp) and face-centered cubic (fcc) phases [14–16]. Qualitatively similar structural phase transitions occur, or are predicted to occur, in other planar systems with varied interparticle interactions, such as plasma dust crystals [17,18], colloidal suspensions [19], semiconductor electron bilayer systems [20] and hard spheres [21]. With a cylindrical geometry, the formation of concentric shells is predicted to occur [22].

The crystallization of small numbers (total number N<50) of laser-cooled ions into Coulomb clusters [23] was first observed in Paul traps [24,25]. With larger numbers of trapped ions, concentric shells [22,26] were directly observed in Penning [27] and Paul traps [6,7,28]. Recently, Bragg diffraction has been used to detect bcc crystals (the predicted infinite volume ordering) in large and spherical (N>2.7 $\times 10^5$, radius $r_0 > 60a_{ws}$) ion plasmas confined in a Penning trap [4,5].

In this paper we present measurements taken from direct images of the central (r=0) structure of pancake-shaped (lenticular) ion plasmas (aspect ratio $\alpha \equiv z_0/r_0 < 0.1$, where $2z_0$ is the plasma center's axial extent). This region has a disk-like geometry with constant central areal density σ_0 (charge density per unit area projected onto the $z = 0$ plane), which facilitates comparison with planar theory. We observed five different stable crystalline phases and found that the energetically favorable central structure could be tuned by changing σ_0. Both continuous and discontinuous structural phase transitions were observed. We also present direct images of the structures observed in small ion clouds which formed cylindrical shells, and in large spherical clouds which produced spatially homogeneous crystals near the cloud center, and compare our results with those of previous workers [4,5,27].

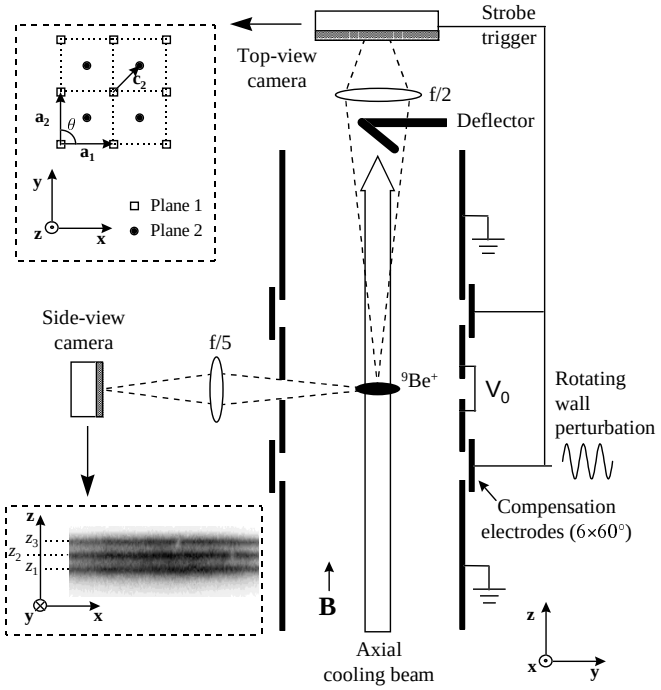

FIG. 1. Schematic side view of the cylindrical Penning trap with its side- and top-view imaging optics. The insets show the variables used to characterize the intra- and interlayer structure. The side-view inset also shows the central region of a lenticular ion plasma with three axial lattice planes.

II. EXPERIMENTAL APPARATUS

The $^9Be^+$ ions were confined radially in a cylindrical Penning-Malmberg trap (Fig. 1, inner trap diameter 40.6 mm) by a uniform magnetic field B=4.465 T in the $\hat{\mathbf{z}}$-axis direction. The ions were confined axially by a potential difference of V_0 (usually -1.50 kV) applied between the center and end electrodes of the trap. Near the trap center this axial potential is quadratic and has a value of $1/2(m/e)\omega_z^2 z^2$, where the axial frequency $\omega_z/2\pi$ = 978 kHz for $^9Be^+$ and V_0 = -1.50 kV. The radial electric fields of the trap, as well as the ion space charge, cause the ion plasma to undergo an $\mathbf{E}\times\mathbf{B}$ drift and thus rotate about the trap axis. In thermal equilibrium, this rotation is at a uniform frequency ω_r. The radial binding force of the trap is determined by the Lorentz force caused by the plasma's rotation through the magnetic field. Thus, low ω_r results in a weak radial binding and a lenticular plasma with a large radius. For 10^4 trapped ions with $\omega_r/2\pi = 68.5$ kHz (typical for our work on planar clouds), the ion plasma has a density of 2.1×10^8 cm^{-3} with $2r_0 \approx 1.3$ mm and an aspect ratio $\alpha \approx 0.05$. The rotation frequency was controlled by phase-locking the plasma rotation to an applied "rotating wall" electric field [29,30]. At low ω_r, an increase in ω_r increases both the plasma density and z_0, providing a way to sensitively adjust σ_0.

The ions were cooled [3] by an axial laser beam propagating along the z axis and tuned 10 to 20 MHz lower in frequency than a hyperfine-Zeeman component of the $2s\ ^2S_{1/2} \rightarrow 2p\ ^2P_{3/2}$ resonance at 313 nm with a natural linewidth of 19 MHz. The laser power was $\sim 50\ \mu$W and was focused at the ion plasma to a diameter of $\sim$ 0.5 mm. There was also a perpendicular cooling beam, derived from the same laser, which had a $\sim 70\ \mu$m waist and a variable power. The theoretical cooling limit is 0.5 mK, and an experimental upper bound of T < 10 mK has been measured [31]; for a density of $n_0 = 2\times10^8$ cm^{-3}, these limits give a range of $160 < \Gamma < 3150$. A series of lenses form side- and top-view images of the ions, with viewing directions perpendicular and parallel to the magnetic field respectively, on either a gateable charge-coupled device (CCD) camera, or on an imaging photomultiplier tube. The resolution of the optical systems is $\sim 4\ \mu$m, while typical interparticle spacings are $\sim 15\ \mu$m.

III. RESULTS AND ANALYSIS

A. Structure in Planar OCPs - 1 to 5 planes

The side-view image inset in Fig. 1 shows the central region of a lenticular ion plasma with three axial lattice planes. It is representative of the flatness and radial extent (<10% of r_0) of the plasma regions used to study the planar OCP. At a large radius, curvature of the planes can cause the side-view images of axial plane positions to blur. This effect was prevented in the planar measurements reported here by using clouds with sufficient amounts (up to 50%) of nonfluorescing impurity ions. Because these heavier-mass ions are centrifugally separated to larger radii than the $^9Be^+$, the regions of the plasma where curvature begins to be significant can be filled with these ions, which are sympathetically cooled by the $^9Be^+$ [32,33].

With good alignment of the trap with the magnetic field (<10^{-3} rad), the ion plasma rotation is phase-locked with the rotating wall perturbation [29,30]. A direct observation of the rotating ion structures was achieved for the first time by gating the top-view CCD camera synchronously with the rotating wall perturbation for brief gate times (< 2% of the plasma rotation period). Total exposure times of $\sim 3\times10^4$ rotation periods were used in typical images (Fig. 2). For our study of the ion lattice structure we limited our analysis to the central region, where strong localization and regular ordering of the ions were observed. At larger radius we observed an increased blurring (due to the plasma rotation), occasional lattice distortions, and, ultimately, the transition to the regions filled by heavier-mass ions.

TABLE I. Primitive and interlayer displacement vectors in (x, y) plane for the observed phases, where $\hat{x} \equiv \mathbf{a_1}/|a_1|$.

Phase	Symmetry	Stacking	Lattice Type	$\mathbf{a_1}$	$\mathbf{a_2}$	$\mathbf{c_2}$	$\mathbf{c_3}$
I	hexagonal	single plane	-	$(a, 0)$	$(a\cos 60^\circ, a\sin 60^\circ)$	–	–
III	square	staggered	bcc (001)	$(a, 0)$	$(0, a)$	$(\mathbf{a_1}+\mathbf{a_2})/\mathbf{2}$	$(0, 0)$
IV	rhombic	staggered	bcc (110)	$(a, 0)$	$(a\cos\theta, a\sin\theta)$	$(\mathbf{a_1}+\mathbf{a_2})/\mathbf{2}$	$(0, 0)$
V	hexagonal	hcp-like	hcp	$(a, 0)$	$(a\cos 60^\circ, a\sin 60^\circ)$	$(\mathbf{a_1}+\mathbf{a_2})/\mathbf{3}$	$(0, 0)$
V_{fcc}	hexagonal	fcc-like	fcc (111)	$(a, 0)$	$(a\cos 60^\circ, a\sin 60^\circ)$	$(\mathbf{a_1}+\mathbf{a_2})/\mathbf{3}$	$2(\mathbf{a_1}+\mathbf{a_2})/\mathbf{3}$

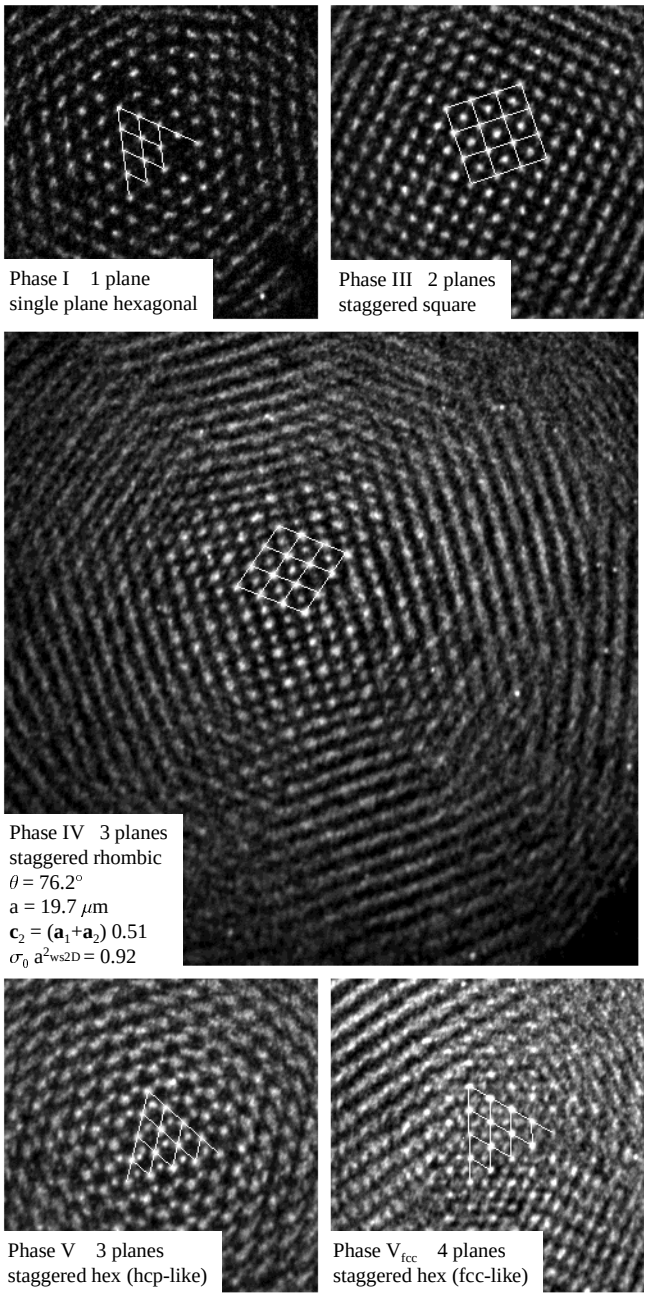

FIG. 2. Top-view (x, y) images of the five structural phases observed in the experiment, with lines showing a fit of the central ions to the indicated structure.

The observed structure of the central crystallized region depended on the central areal density σ_0 of the plasma. Within a layer, the lattice is characterized by the primitive vectors $\mathbf{a_1}$ and $\mathbf{a_2}$ (which are observed to be equal in magnitude, $|\mathbf{a_1}| = |\mathbf{a_2}| \equiv a$), or, equivalently, by a and the angle θ ($\leq 90^\circ$) between the primitive vectors. The interlayer structure is characterized by the axial positions z_n of the n lattice planes (measured by the side-view camera) and the interlayer displacement vector $\mathbf{c_n}$ between layers 1 and n. (These variables are shown in the inset of Fig. 1.) Hence, the equilibrium (x, y) positions of ions in axial planes 1 and n are given by $\mathbf{R_1}(i, j) = i\mathbf{a_1} + j\mathbf{a_2}$ and $\mathbf{R_n}(i, j) = i\mathbf{a_1} + j\mathbf{a_2} + \mathbf{c_n}$, where i, j are integers.

Three different types of intralayer ordering were observed: hexagonal ($\theta = 60^\circ$), square ($\theta = 90^\circ$) and rhombic ($90^\circ > \theta \geq 65^\circ$). The square and rhombic layers stack in a staggered fashion, with the upper ions immediately above the centers of the parallelograms below, resulting in an interlayer displacement vector $\mathbf{c_2} = (\mathbf{a_1} + \mathbf{a_2})/2$. Hexagonal layers also stack with ions above the centers of the triangles below, but this stacking can occur in two distinct ways: $3\mathbf{c_2} = \mathbf{a_1} + \mathbf{a_2}$ and $3\mathbf{c_2}/2 = \mathbf{a_1} + \mathbf{a_2}$. With hcp-like stacking, the ions in every other plane lie directly above each other (*abab...*), while with fcc-like stacking, the ions in every third plane are so aligned (*abcabc...*). When there were 3 or more hexagonal layers, both types of stacking were observed.

The following sequence of phase structures, with their lattice parameters and types defined in Table 1, were observed as the central areal density σ_0 was increased from where order was first observed: (I) one-layer hexagonal $\rightarrow$ (III) two-layer staggered square $\rightarrow$ (IV) two-layer staggered rhombic $\rightarrow$ (V) two-layer staggered hexagonal. At a critical density, a third layer was formed, resulting in a (III) three-layer staggered square. The process then repeated with minor variations, such as phase III becoming less common. We have followed the classifications used in previous theoretical studies of quantum [20,34] and classical [16] electron bilayer systems. Phase II, which is a stable phase of the bilayer systems where the interlayer distance is fixed, is not listed here because it is unstable for the planar OCP, where this distance can vary.

We have performed an analytical calculation of the energies of these phase structures for the planar OCP. The

theory uses Ewald summation techniques in order to minimize the energy of n parallel lattice planes confined in a harmonic potential of the form $\phi_e = 1/2(m/e)\omega_z^2 z^2$. Because this potential is identical to the confinement potential of a Penning trap in the $\alpha \to 0$ planar limit [35], the theory should predict the structures that are observed in the central region of the plasmas of the experiment. However, since only minimum energy states are determined, the theory provides the lattice structure only for the case of zero temperature ($\Gamma = \infty$).

The energy minimization was performed holding fixed the total number of ions per unit area, σ. In order to make the analysis tractable, each lattice plane was assumed to have the same structure, consisting of a 2D lattice described by primitive vectors $\mathbf{a_1}$ and $\mathbf{a_2}$. Since the area of the 2D primitive cell, $a_1 a_2 \sin\theta$, is fixed to the value n/σ by the constraint that σ is fixed, the parameters that were varied in order to minimize the energy were a_2/a_1, θ, $\mathbf{c_n}$ and z_n. The functional form of the energy is given in ref. [36].

There were several local minima in the energy function, corresponding to different minimum energy lattices. A numerical search was performed to find the true global minimum with respect to the above-listed parameters. Finally, the search was repeated for several values of n at a given value of σ, and the value of n that provides the lowest energy is kept. The search was then repeated for a range of values of σ.

We found that, just as in the experiments, the minimum energy state had one of 4 separate topologies, depending on the value of σ. The structures are listed in Table 1 as phases I, III, IV, and V_{fcc}. In addition, there was a fifth hcp phase, phase V, which was stable and had only slightly higher energy than phase V_{fcc}.

The rhombic phase, phase IV, was missed in two previous publications on the minimum energy states of this system [15,36]. This is because the previous publications did not perform a full numerical minimization with respect to all of the parameters of the model. Instead, only phases I, III, V and V_{fcc}, along with a few other symmetric phases, were considered. Although stability of these phases was checked by evaluating the normal modes of the lattices, it was not recognized that phase III becomes unstable to the rhombic phase IV deformation, since this instability was suppressed by the periodic boundary conditions. Fortunately, the energy of the rhombic phase is only slightly lower than that of phase III so the conclusions of the previous works concerning the phase diagram of the system are only slightly altered. In particular, the maximum size of approximately 60 lattice planes required to observed bulk bcc behavior is unaffected [37].

The predictions of the analytic planar OCP theory, which has no free parameters, were compared directly with the observations by identifying σ, the areal density of the planar OCP, with the directly measured central areal density σ_0 of the lenticular plasmas. For a quantitative analysis of the observed lattice structure, we performed a least squares fit of the positions of the ions in the central region to the relevant phases (shown in Table I) (lines in Fig. 2). Using the best-fit values of the primitive vector length a and the intralayer angle θ and the observed number of lattice planes n, we calculated the central areal density $\sigma_0 = n/(a^2 \sin\theta)$.

The agreement between the planar OCP theory and experiment, with measurements taken on different plasmas with N$< 10^4$, is good (Fig. 3). As the central areal density was increased, the lattice planes moved further apart axially (Fig. 3a). Eventually, it became energetically favorable to form an additional lattice plane. How-

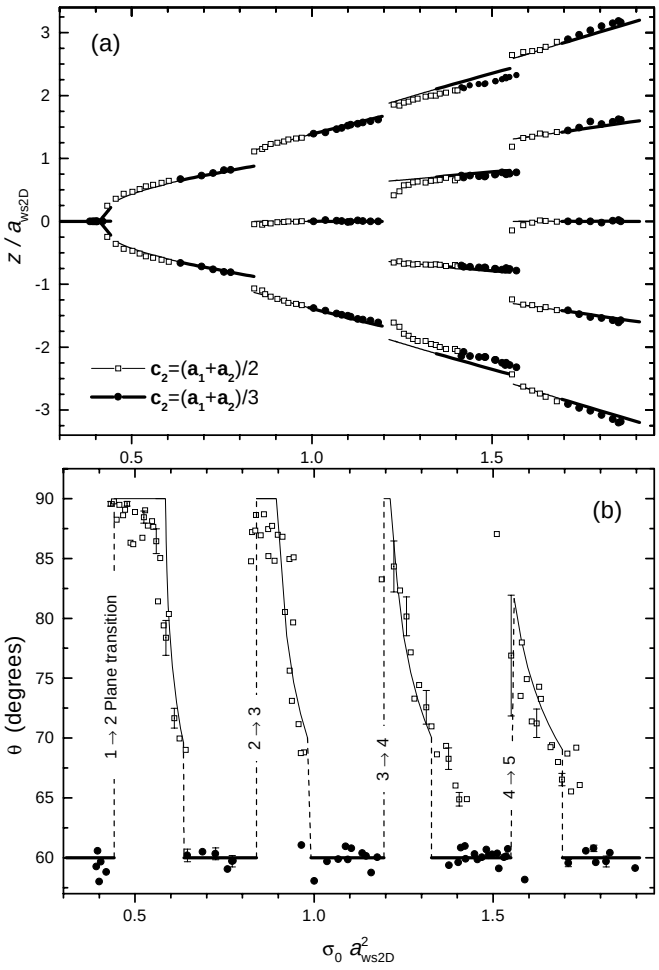

FIG. 3. (a) Interlayer structure (plane axial positions and displacement vectors) and (b) intralayer angle θ of the central region as a function of central areal charge density. The lines show predictions from theory, and symbols show experimental measurements. Also indicated is whether the lattices have an interlattice displacement vector $\mathbf{c_2}$ characteristic of the hexagonal phases (circles, thick lines) or the square and rhombic phases (squares, thin lines). Lengths have been normalized by $a_{ws2D} = (3e^2/4\pi\epsilon_0 m\omega_z^2)^{1/3} = 10.7$ μm, which is the Wigner-Seitz radius in the planar limit.

ever, although the phase V_{fcc} was predicted to be slightly more energetically favorable than phase V, we rarely observed V_{fcc} ($\sim 10\%$ of the time). These and other minor discrepancies from theory may be due to the finite radial extent or the non-zero temperature of the ion plasma; we observed a similar preference for hcp stacking in molecular dynamics simulations of small (N=3000) lenticular ion plasmas with $\Gamma = 500$.

For the dependence of the angle θ (between the primitive vectors $\mathbf{a_1}$ and $\mathbf{a_2}$) on central areal density σ_0 (Fig. 3b), the general trend was that, when a new lattice plane was formed, θ changed discontinuously from $\sim 60°$ to a higher value. As σ_0 of the crystal was further increased, θ smoothly decreased to $\approx 65°$ until there was a second discontinuous transition to a hexagonal structure. This second transition has been predicted to become continuous, with θ assuming all values $60° \leq \theta \leq 90°$, in liquid ($\Gamma < 80$) bilayer systems [38]. The lines indicate the minimum energy structures predicted by the analytic theory. At central areal charge densities near phase boundaries, both phases could be observed. In these regions, the phase which materialized after the crystal was formed was initially random, but tended to persist if the ions were not heated. Where there was not a strong preference for one phase over the other, both were plotted.

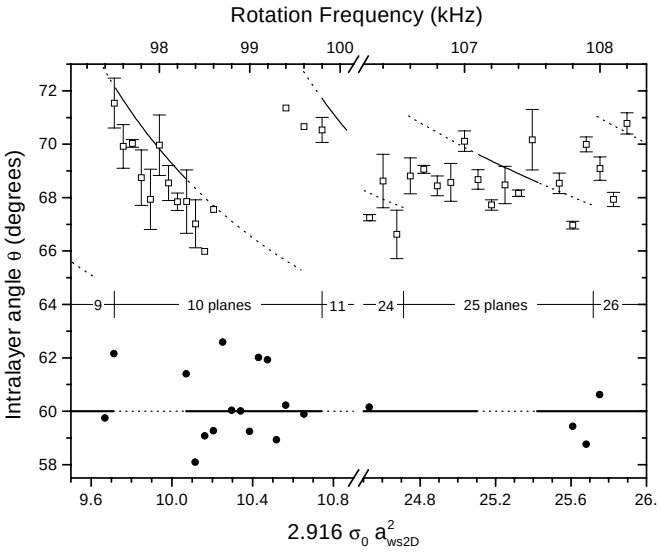

FIG. 4. Intralayer angle θ of the central region for 2 ion plasmas with $9 \rightarrow 11$ planes (left) and $24 \rightarrow 26$ planes (right). The symbols are experimental measurements plotted versus rotation frequency. The lines are from the T=0 theory, with dashes indicating that the structure is not predicted to be energetically favorable.

B. Structure in Planar OCPs - 5 to 45 planes

By increasing the number of lattice planes we have been able to study the transition from the several plane regime where surface energy contributions are important, to one where bulk energy contributions become more important. The basic result as we increased the number of planes is that bands of alternating phase IV (bcc-like) and phases V and V_{fcc} (fcc-like) were observed, until above ~ 30 planes where phase IV with θ within a few degrees of 70° was exclusively seen. When $\theta = 70.53°$, phase IV is equivalent to bcc ordering (with a (110) alignment), which is the predicted infinite volume ordering.

The increased axial extent of the plasmas required a modification in how the images of structure were obtained. For plasmas with $2z_0$ greater than the depth of field of the top-view f/2 objective lens (~ 80 μm), the cooling-laser beam directed perpendicularly to $\mathbf{B}$ was used to illuminate a section of the plasma within the depth of field (see Figs. 5b and 6 below). The fluorescence from the ions outside this region illuminated by the parallel beam could be made negligible by chopping the parallel beam with an optical wheel and gating the CCD camera on only when the parallel beam was blocked. This chopping technique was also occasionally used with the side-view images in order to improve their spatial resolution.

Figure 4 plots the measured and predicted intralayer angle θ of the central regions, for parameters near where the plasma has 10 and 25 axial lattice planes. Because the experimental uncertainties in a and θ cause the calculated σ_0 to have an unacceptably large scatter for large number of planes, the experimental measurements have been plotted as a function of the plasma rotation frequency, which increases monotonically with σ_0. To match the observations with the theory, the range of the plotted rotation frequencies (top axis) was adjusted to make the points where the $9 \rightarrow 10$, $10 \rightarrow 11$, $24 \rightarrow 25$ and $25 \rightarrow 26$ transitions were observed coincide with the theory predictions.

Good agreement with the analytic theory continued to be seen with 10 planes: Phases IV and V or V_{fcc} alternated as the energetically preferred structure, and the intralayer angle θ of phase IV showed the expected decrease as the central areal density of the crystal is increased. With larger numbers of planes, however, phase IV was observed to occur more often than predicted (Table II). A plausible explanation for why this occurs is finite temperature effects. Dubin and O'Neil [37] have determined the free energy of various lattice types for the planar OCP as a function of both σ and Γ. In Fig. 9 of [37] they plot which of the two main lattices, fcc (111) and bcc (110), has the lower free energy for the regimes $200 < \Gamma < 5000$. They found that as Γ was decreased, the areal density above which the bcc(110) phase is exclusively favored decreases. For example, for $\Gamma = 600$ bcc (110) is exclusively favored when $n > 30$.

TABLE II. Incidence of Phase IV in Planar OCPs.

Number of Planes	Experiment (%)	T=0 Theory (%)
5	50	40
10	52	35
20	76	31
25	90	31
33	>97	26
45	>97	34
60		100

C. Shell Structure in Small OCPs

When the rotation frequency is increased the plasma changes shape from oblate to prolate, and the lattice planes near the plasma boundary bend in order to conform with the curvature of the boundary. The minimum energy structure at these regions consists of concentric shells each made up of imperfect 2D hexagonal crystal sheets [22,26]. The shell curvature results in a loss of correlation between shells since the 2D lattices on different shells get "out of phase" as one moves from point to point on the shell surfaces [37]. With small plasmas where boundary effects are important, shell structure can be the minimum energy structure of the cloud; that is, the shell structure exists throughout the interior as well as near the plasma boundary.

Shell structure has been previously imaged in both Penning and rf trap experiments [7,27,28]. In the Penning trap experiment, some differences with the simulations were observed. In particular the shells were frequently observed to be open ended cylinders (parallel to the $\hat{z}$-axis) rather than the predicted closed spheroidal shells. In order to investigate this discrepancy with the present trap, which includes the capability of taking side-view images, we returned to the geometry of the previous experiments. Figure 5 shows side (a) and top-view (b) images of shell structure obtained on a plasma of N=9000 Be^+ ions and 15,000 impurity ions. Neither image was strobed with the rotating wall perturbation.

In Fig. 5(a) the parallel beam was chopped at a 1 kHz rate and the sideview camera was gated on only when the parallel beam was gated off. The perpendicular laser beam was then translated up and down throughout the plasma and the resultant ion fluorescence was integrated over many translations of the beam, producing a slice of the shell structure cutting through the plasma near the r=0 axis. The viewing optics are at 60° with respect to the perpendicular beam (Fig. 5(c)), which, along with the small offset of the beam from the $r = 0$ axis, produced an image where the shell structure was well defined on the right hand side of 5(a). In Fig. 5(b) the perpendicular laser beam was held fixed near the central (z=0)

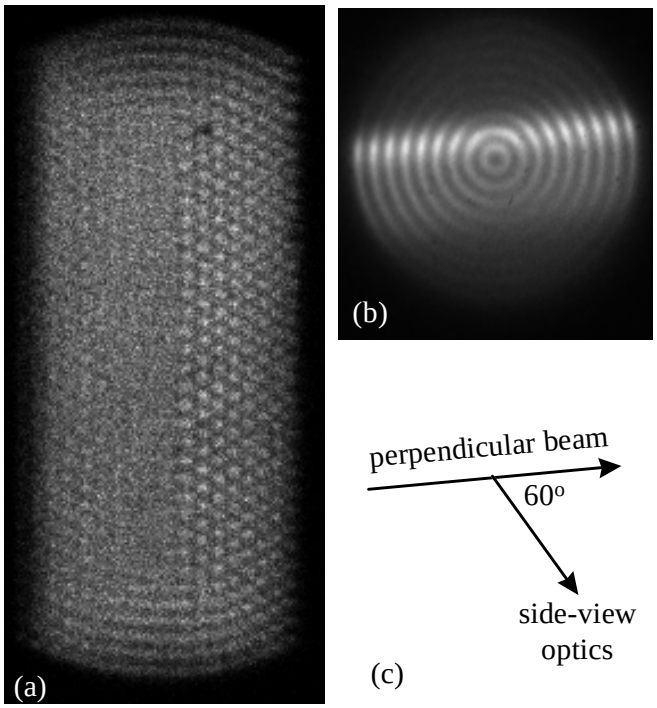

FIG. 5. Side-view (a) and top-view (b) images of an ion cloud with rotation frequency $\omega_r = 2\pi$ 63 kHz confined into a cylindrical shape due to the presence of centrifugally separated heavier mass impurity ions. The viewing angle of the side-view optics is shown (top-view) in (c).

section of the plasma and the ion fluorescence produced by both the parallel and perpendicular laser beams were integrated on the top-view camera. However, because the camera was also focussed on the central section of the plasma, this figure essentially shows a cross section of the shell structure near z=0.

The ion plasma of Fig. 5 had 9 shells that were cylindrical near the middle (z=0) section of the plasma. The cylindrical shells were produced by the presence of heavier mass contaminant ions, which centrifugally separated and produced a cylindrical boundary to the lighter Be^+ ions. Figs. 5(a) and 5(b) show resolved spatial structure in the axial and radial directions, respectively. However, in agreement with the simulations, the cylindrical shells are not open-ended, but are closed by curved shell structure. The curvature of the shells near the ends of the plasma was also observed in top-view images like Fig. 5(b) when the perpendicular laser beam was directed near an axial end of the plasma. The reason for the frequent observation of open-ended cylindrical shells in the earlier Penning trap experiments is unknown, as we were not able to produce open-ended cylindrical shells in this work. For example, misaligning the trap symmetry axis with the magnetic field by up to 3×10^{-4} rad had no apparent effect on the shell structure.

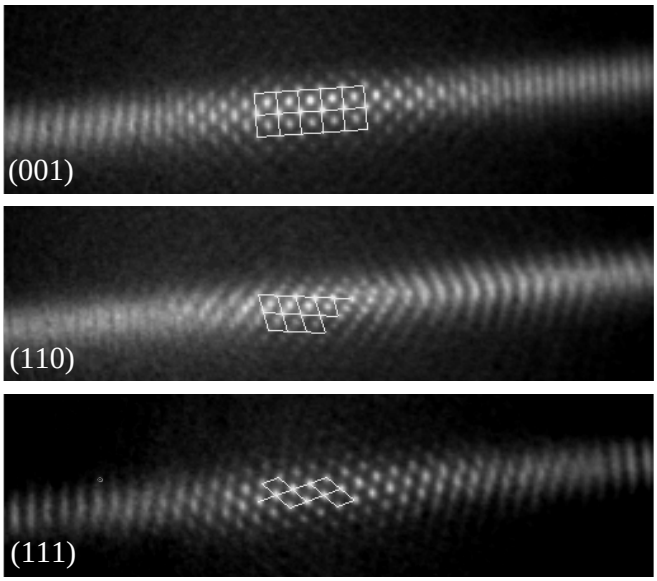

FIG. 6. Top-view images of a spherical cloud with 100,000 Be^+ ions and 60,000 impurity ions, with lines showing a fit to bcc lattice structure with the indicated orientation. The length and axial extent of the perpendicular beam in the image are 60 and 8 a_{ws}, respectively.

D. Crystal Structure in Large OCPs

The formation of structure in spherical plasmas with large numbers of ions has been studied experimentally using Bragg diffraction [4,5]. Long-range order (crystallization) was found to emerge in plasmas with N > 50,000 ions (radius $r_0 \approx 37a_{ws}$), consistent with simulations of a 20,000 ion spherical plasma which found only short range order in the form of approximately 20 spherical shells [39]. Bulk behavior (bcc crystals exclusively) was observed in plasmas with N > 270,000 ($r_0 \approx 60a_{ws}$), and lower limits to the crystal diameters of 17 and 28 a_{ws} were estimated from the widths and intensities of the Bragg peaks, respectively.

We have used top-view images, strobed by the rotating wall perturbation, of a large (N $\sim$ 160,000, $r_0 \approx 50\ a_{ws}$) ion cloud to further investigate structure in this regime. Figure 6 shows examples of such images, along with lines showing a fit to a bcc lattice structure. Both bcc and fcc structure were observed, with bcc occurring $\sim$ 70% of the time. A variety of orientations was observed, but these were usually consistent with symmetry axes of the crystal, suggesting that there were boundary conditions such as the presence of impurity ions which prevent completely random orientations of the crystal. Evidence for preferred orientations has been previously noted [5].

The region with the strongest localization of individual ions was found to be a cylinder along the $r = 0$ axis of the plasma. A typical diameter was $\sim$ 16 a_{ws}, and it extended axially throughout the sphere until significant curvature of the end planes was encountered. The transition from crystal structure to concentric shells was not abrupt, as can be seen in Fig. 6 where the structure observed out to $r = 30a_{ws}$ from the center is not regularly spaced.

IV. DISCUSSION

With spatial imaging, we have measured the correlations of strongly coupled $^9Be^+$ ion plasmas in a variety of different geometries. The planar geometry in particular permits a detailed comparison with theoretical calculations, and in general the agreement between the observations and theory is good. We have measured the energetically preferred structures in lenticular plasmas for up to 45 lattice planes and find a transition from surface-dominated to bulk behavior to occur when the ion plasma is $\sim$ 30 planes in axial extent. Ions in a trap have been proposed as a register for a quantum computer [40]. Work in this area has focussed on a string of a few ions in a linear Paul trap [41]. A single lattice plane of ions as shown in Fig. 2 could provide an alternative 2D geometry of trapped ions for studies of quantum computing or entangled quantum states.

In large and spherical plasmas, we have observed the formation of crystals with long range order. The crystals occupied the inner cylindrical core of the plasma, and their orientation appeared to be influenced by external perturbations since it was not completely random. Outside the crystal there was a complicated transition to shell structure. We have not observed the thermodynamic liquid-solid phase transition predicted for the bulk OCP, as our measurements have concentrated on the correlations obtained at the coldest temperatures (therefore maximum Γ) where the ion fluorescence is maximum. The study of this phase transition in the bulk and 2D geometries my be an interesting direction for future studies with this system.

ACKNOWLEDGMENTS

This research was supported by the Office of Naval Research and the National Science Foundation (D. H. E. D.). We thank D. J. Wineland for useful comments, and B. M. Jelenković and J. N. Tan for technical assistance. This manuscript is a work of the U.S. government; it is not subject to U.S. copyright.

[1] H. M. Van Horn, Science **252**, 384 (1991).

[2] C. C. Grimes and G. Adams, Phys. Rev. Lett. **42**, 795 (1979).
[3] D. J. Wineland, R. E. Drullinger, and F. L. Walls, Phys. Rev. Lett. **40**, 1639 (1978).
[4] J. N. Tan, J. J. Bollinger, B. Jelenković, and D. J. Wineland, Phys. Rev. Lett. **75**, 4198 (1995).
[5] W. M. Itano *et al.*, Science **279**, 686 (1998).
[6] I. Waki, S. Kassner, G. Birkl, and H. Walther, Phys. Rev. Lett. **68**, 2007 (1992).
[7] G. Birkl, S. Kassner, and H. Walther, Nature **357**, 310 (1992).
[8] T. B. Mitchell *et al.*, Science **282**, 1290 (1998).
[9] P. K. Ghosh, *Ion Traps* (Clarendon, Oxford, 1995).
[10] *Non-Neutral Plasma Physics*, edited by C. W. Roberson and C. F. Driscoll (AIP, New York, 1988).
[11] S. Ichimaru, H. Iyetomi, and S. Tanaka, Phys. Rep. **149**, 91 (1987).
[12] G. S. Stringfellow and H. E. DeWitt, Phys. Rev. A **41**, 1105 (1990).
[13] D. H. E. Dubin, Phys. Rev. A **42**, 4972 (1990).
[14] J. P. Schiffer, Phys. Rev. Lett. **70**, 818 (1993).
[15] D. H. E. Dubin, Phys. Rev. Lett. **71**, 2753 (1993).
[16] G. Goldoni and F. M. Peeters, Phys. Rev. B **53**, 4591 (1996).
[17] J. B. Pieper, J. Goree, and R. A. Quinn, J. Vac. Sci. Technol. A **14**, 519 (1996).
[18] H. Totsuji, T. Kishimoto, and C. Totsuji, Phys. Rev. Lett. **78**, 3113 (1997).
[19] D. H. Van Winkle and C. A. Murray, Phys. Rev. A **34**, 562 (1986).
[20] S. Narasimhan and T.-L. Ho, Phys. Rev. B **52**, 12291 (1995).
[21] M. Schmidt and H. Löwen, Phys. Rev. E **55**, 7228 (1997).
[22] A. Rahman and J. P. Schiffer, Phys. Rev. Lett. **57**, 1133 (1986).
[23] R. Rafac *et al.*, Proc. Natl. Acad. Sci. USA **88**, 483 (1991).
[24] F. Diedrich *et al.*, Phys. Rev. Lett. **59**, 2931 (1987).
[25] D. J. Wineland *et al.*, Phys. Rev. Lett. **59**, 2935 (1987).
[26] D. H. E. Dubin and T. M. O'Neil, Phys. Rev. Lett. **60**, 511 (1988).
[27] S. L. Gilbert, J. J. Bollinger, and D. J. Wineland, Phys. Rev. Lett. 2022 (1988).
[28] M. Drewsen *et al.*, Phys. Rev. Lett. **81**, 2878 (1998).
[29] X.-P. Huang, J. J. Bollinger, T. B. Mitchell, and W. M. Itano, Phys. Rev. Lett. **80**, 73 (1998).
[30] X.-P. Huang, J. J. Bollinger, T. B. Mitchell, and W. M. Itano, Phys. Plasmas **5**, 1656 (1998).
[31] L. R. Brewer *et al.*, Phys. Rev. A **38**, 859 (1988).
[32] T. M. O'Neil, Phys. Fluids **24**, 1447 (1981).
[33] D. J. Larson *et al.*, Phys. Rev. Lett. **57**, 70 (1986).
[34] G. Goldoni and F. M. Peeters, Europhys. Lett. **37**, 293 (1997).
[35] T. M. O'Neil and D. H. E. Dubin, Phys. Plasmas **5**, 2163 (1998).
[36] D. H. E. Dubin, Phys. Rev. A **40**, 1140 (1989).
[37] D. H. E. Dubin and T. M. O'Neil, in *Strongly Coupled Plasma Physics*, edited by S. Ichimaru (Elsevier/Yamada, Osaka, 1990), p. 189.
[38] V. I. Valtchinov, G. Kalman, and K. B. Blagoev, Phys. Rev. E **56**, 4351 (1997).
[39] J. P. Schiffer, in *Non-Neutral Plasma Physics II*, edited by J. Fajans and D. H. E. Dubin (AIP, New York, 1995), p. 191.
[40] J. I. Cirac and P. Zoller, Phys. Rev. Lett. **74**, 4091 (1995).
[41] D. J. Wineland *et al.*, J. Res. Natl. Inst. Stand. Technol. **103**, 259 (1998).